Shear-induced grain boundary motion for lamellar phases in the weakly nonlinear regime

Zhi-Feng Huang* and Jorge Viñals†
School of Computational Science and Information Technology, Florida State University, Tallahassee, Florida 32306-4120, USA
(Received 6 November 2003; published 30 April 2004)

We study the effect of an externally imposed oscillatory shear on the motion of a grain boundary that separates differently oriented domains of the lamellar phase of a diblock copolymer. A direct numerical solution of the Swift-Hohenberg equation in shear flow is used for the case of a transverse/parallel grain boundary in the limits of weak nonlinearity and low shear frequency. We focus on the region of parameters in which both transverse and parallel lamellae are linearly stable. Shearing leads to excess free energy in the transverse region relative to the parallel region, which is in turn dissipated by net motion of the boundary toward the transverse region. The observed boundary motion is a combination of rigid advection by the flow and order parameter diffusion. The latter includes break up and reconnection of lamellae, as well as a weak Eckhaus instability in the boundary region for sufficiently large strain amplitude that leads to slow wave number readjustment. The net average velocity is seen to increase with frequency and strain amplitude, and can be obtained by a multiple scale expansion of the governing equations.

DOI: 10.1103/PhysRevE.69.041504 PACS number(s): 83.50.−v, 47.54.+r, 05.45.−a, 61.25.Hq

I. INTRODUCTION

Below an order-disorder temperature, nanoscale phases of various symmetries can be found in block copolymer melts [1,2]. For example, for diblock copolymers that consist of two chemically distinct but covalently bonded monomers, six distinct phases that result from microphase separation have been documented [1]. They differ by the symmetry of their composition modulation. One of the most actively investigated microphases is the lamellar phase, which can be observed around 50-50 composition (symmetric mixture). However, when melts are processed by thermal quenching or solution casting from a disordered phase, a macroscopic size sample usually exhibits polycrystalline configurations comprising many locally ordered but randomly oriented domains (grains) and large amounts of topological defects, such as grain boundaries, dislocations, and disclinations. Such state of partial ordering is undesirable for many applications, with significant effects on, e.g., the optical and mechanical performance of the material. Therefore, the realization and control of long-range orientational order of domains has been of great interest in both experimental and theoretical studies.

Several methods have been used experimentally to achieve microstructural alignment in block copolymer melts since the discovery of flow-induced alignment by Keller *et al.* [3]. One of the most common ways to induce global order in bulk samples is to impose an oscillatory or steady shear between two parallel plates, which not only has the advantage of easily characterizing the shear stress and monitoring the aligning progress, but also can bring some interesting new physics [1,2,4–9]. For the case of lamellar morphology that we are interested in here, the two most often observed alignments relative to the imposed shear are parallel (with the lamellar layers parallel to the shearing plane) and perpendicular (with the lamellar layers normal to the vorticity of the shear flow). Both alignments have been observed in nearly symmetric diblock copolymer systems such as poly(ethylenepropylene)-poly(ethylethylene) (PEP-PEE) [5] and polystyrene-polyisoprene (PS-PI) [6,7]. Which of these two possible alignments is selected in a given experiment depends on temperature, and shear strain amplitude and frequency [2,8,9]. A third alignment direction, the so-called transverse orientation in which the lamellar normal is parallel to the shear direction, has been found to coexist with parallel orientation for entangled poly(styrene-b-ethylenepropylene) (S-EP) diblock copolymer at high frequency and in the strong segregation limit [10]. Other studies have focused on the kinetics of global alignment and have shown that the ordering rate increases with shear frequency, strain amplitude, and temperature [8,11]. Experiments on PS-PI diblocks further show nonlinear effects of the strain amplitude on the alignment rate, and that the time scale for the development of alignment exhibits a power law dependence on the strain amplitude, with an exponent equal to −3 or −5, depending on the stage of alignment and in different frequency regimes [11]. Furthermore, many experiments have indicated that the motion of topological defects plays an important role in the global alignment of microdomains under shear, including the evolution of kink band defects and tilt boundaries [12], as well as the migration and annihilation of partial focal conic defects, boundaries, and tilt walls [8,13].

A coarse-grained description of a diblock copolymer melt has been used, both in the weak segregation [14–16] and strong segregation [15] regimes, to theoretically understand the effect of shear flow and the mechanisms of morphology evolution [17–24]. The analytic studies of Cates and Milner [17], and Fredrickson [18] focused on the order-disorder transition from the isotropic state to the lamellar phase and the related alignment dynamics for systems subjected to steady shear flow. Below the transition temperature, the stability of uniform lamellar structures under an oscillatory shear flow has been addressed in both two-dimensional (2D)

*Electronic address: huang@csit.fsu.edu
†Electronic address: vinals@csit.fsu.edu

[19] and three-dimensional (3D) [20] cases. Bifurcation diagrams, including secondary instabilities (Eckhaus and zigzag), were given. These analyses found that although all three types of lamellar orientations could be linearly stable under specific conditions, the stability range of the perpendicular orientation is larger than that of the parallel one, which in turn is larger than the region of stability of the transverse orientation. The perpendicular alignment was also shown to be the preferred orientation following the decay of unstable parallel or transverse lamellae. In addition to these analytic works, computer simulations have been performed to investigate the dynamics of lamellar alignment in bulk samples under steady [21,22,25] or oscillatory [21,23,26] shear flow. The effects of strain amplitude and shear frequency on the degree of sample alignment have been examined, as well as annihilation processes of defects (such as dislocations and disclinations) [23]. Also, domain coarsening in 2D diblock copolymer melts has been addressed although in the absence of shear [27–30]. Little is known about the effect of shear on coarsening of block copolymers.

Few of the previous theoretical studies discussed above focused on the detailed dynamics and quantitative properties of topological defects motion under shear, which are crucial for the understanding of alignment and coarsening. In this paper we study the detailed mechanisms of grain boundary motion under an oscillatory shear flow building upon stability results of uniform lamellar patterns [19,20]. We use a simplified 2D configuration which involves only two lamellar domains of parallel and transverse orientations, respectively, separated by a grain boundary, and focus on shears of small amplitude (less than 50 %) and low angular frequency. Compared to previous numerical simulations [21–23,25–30], the aspect ratio (defined as the ratio between the lateral extent of the system and the lamellar wavelength) is larger, so that important dynamic features associated with grain boundary motion, such as diffusive relaxation of lamellae, phase shift of boundary velocity, and wave number adjustment in the transverse region, can be quantitatively analyzed. These features were absent in earlier work on lamellar (roll) systems without shear [31–35], and we argue below that they are important when the system is under oscillatory shear.

This paper is organized as follows. In Sec. II we introduce a dimensionless model equation based on the Swift-Hohenberg equation to describe the dynamic evolution of symmetric diblock copolymer melts under shear, and describe the grain boundary configuration used. The numerical results including grain boundary velocity and lamellar wave number are presented in Sec. III. We derive amplitude equations governing the system evolution in Sec. IV and compare the results with the direct solutions of Sec. III. Finally, in Sec. V, we summarize our results and discuss the physical origin of the phenomena observed.

II. MODEL EQUATION AND GRAIN BOUNDARY CONFIGURATION

The system under consideration is a symmetric diblock copolymer melt below the order-disorder transition temperature T_{ODT}. For length scales larger than the microscopic monomer scale (i.e., at a mesoscopic level) and time scales long enough compared to the molecular relaxation of the polymer chains, a coarse-grained description of the block copolymer melt can be used, with an order parameter field $\psi(\mathbf{r},t)$ representing the local density difference of the two constituent monomers. In the weak segregation limit, i.e., close to T_{ODT}, a coarse-grained free-energy functional has been derived [14–16]:

$$F[\psi]=\int d\mathbf{r}\left\{-\frac{\tau}{2}\psi^2+\frac{u}{4}\psi^4+\frac{\xi}{2}[(\nabla^2+q_0^{*2})\psi]^2\right\}, \qquad (1)$$

where τ denotes a reduced temperature variable which is a measure of the distance from the order-disorder transition and is positive below T_{ODT}, and $q_0^*=2\pi/\lambda_0^*$ is the wave number of the periodic lamellar structure. Under the assumption that changes in the local composition field ψ are driven by the free-energy minimization and advection by the flow, the order parameter $\psi(\mathbf{r},t)$ obeys a time-dependent Ginzburg-Landau equation

$$\frac{\partial\psi}{\partial t}+\mathbf{v}\cdot\boldsymbol{\nabla}\psi=-\Lambda\frac{\delta F}{\delta\psi}, \qquad (2)$$

where $\mathbf{v}$ is the local velocity field. Because of the emergence of a lamellar phase of finite wave number q_0^*, long-range diffusion is negligible [36], so that the operator $-M\nabla^2$ that corresponds to conserved dynamics for the order parameter ψ in Eq. (2) is approximated by an Onsager kinetic coefficient $\Lambda=Mq_0^{*2}$, with M as mobility. In addition, this equation is only valid for a symmetric diblock for which the spatial average of the order parameter $\bar{\psi}=0$.

We introduce a length scale $1/q_0^*$, a time scale $1/\Lambda\xi q_0^{*4}$ (which is the characteristic polymer relaxation time and $\simeq 1/Dq_0^{*2}$, with D the chain diffusivity of the copolymer), and an order parameter scale $(\xi q_0^{*4}/u)^{1/2}$. Given PEP-PEE-2 as an example, we have $\lambda_0^*\sim 30$ nm, $D\sim 10^{-11}$ cm^2/s for temperatures close to T_{ODT}, and hence the length scale here is about 5 nm and the time scale is about 0.03 s. Consequently, the rescaled composition field ψ obeys a dimensionless Swift-Hohenberg equation [37] with an advection term

$$\frac{\partial\psi}{\partial t}+\mathbf{v}\cdot\boldsymbol{\nabla}\psi=\epsilon\psi-(\nabla^2+q_0^2)^2\psi-\psi^3, \qquad (3)$$

where $\epsilon=\tau/\xi q_0^{*4}$ and we have $0<\epsilon\ll 1$ in the weak segregation regime considered here. Also, $q_0=1$ although the symbol q_0 is retained in what follows for clarity of presentation.

As shown in Fig. 1, we consider a 2D reference state below the order-disorder transition containing a planar grain boundary that separates two semi-infinite ordered domains A and B. Initially both domains are in the lamellar state with the same wave number q_0 but oriented along different directions. We are interested here in the case of a 90° grain boundary with two mutually perpendicular lamellar sets A and B, a configuration that is known to be stable against small perturbations in the absence of shear [32–34]. The two domains are under an imposed shear flow

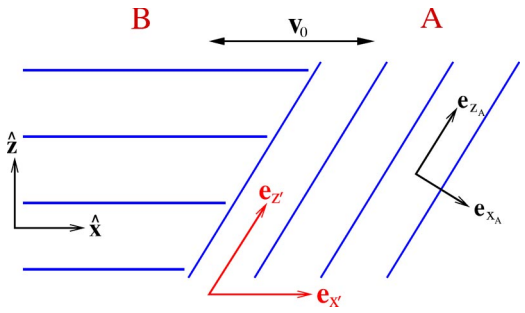

FIG. 1. Schematic representation of the two-dimensional grain boundary configuration under oscillatory shear flow studied in this paper. Both the nonorthogonal sheared frame $\{\mathbf{e}_{x'},\mathbf{e}_{z'}\}$, and the auxiliary frame $\{\mathbf{e}_{x_A},\mathbf{e}_{z_A}\}$ are indicated.

$$\mathbf{v}_0 = \frac{da}{dt} z\hat{\mathbf{x}} = \gamma\omega \cos(\omega t) z\hat{\mathbf{x}}, \tag{4}$$

where da/dt represents the shear rate with strain $a(t) = \gamma \sin(\omega t)$, ω is the angular frequency, γ the strain amplitude, and all quantities are assumed dimensionless. Lamellae of domain A are transverse (with the wave vector components $q_x = q_0$ and $q_z = 0$) at $t = 0$, and those in region B parallel ($q_x = 0$ and $q_z = q_0$). Parallel lamellae B are marginal to the shear and not distorted, while transverse lamellae A are compressed, with both orientation and wavelength changing following the imposed shear as shown schematically in Fig. 1. Thus, we anticipate that the grain boundary will not remain stationary even though both A and B lamellae are linearly stable under shear. Net motion results from the free-energy difference between region A (compressed) and region B (unchanged), as well as diffusive relaxation of the order parameter as shown below.

The stability of a uniform configuration of either parallel or transverse lamellae under shear flow has been given in Refs. [19,20]. There exists a critical strain amplitude γ_c above which the lamellar structure of a given orientation melts, with $\gamma_c \to \infty$ for parallel lamellae of wave number $q = q_0$, and small γ_c for transverse orientation. The stability diagrams presenting secondary instability boundaries (for zigzag and Eckhaus modes) for 2D system have also been given in Ref. [19]. We focus below solely on shears for which both uniform parallel and transverse lamellae are linearly stable. In addition, we consider the case in which shear effects are of the same order of magnitude as diffusive relaxation of the order parameter. Otherwise, at one extreme lamellae are passively advected by the flow, whereas at the other, diffusion dominates. If the velocity $\mathbf{v}$ in Eq. (3) can be approximated as $\mathbf{v}_0$ (which is the case under certain conditions [18], including neglecting back flows due to osmotic stresses, and any viscosity contrast between the microphases), then the interesting range of γ is such that the advection contribution due to the imposed shear [$\mathbf{v}\cdot\nabla = (da/dt) z\partial_x$ in Eq. (3)] is $O(\epsilon)$. As will be further discussed in Sec. IV in connection with our multiple scale analysis, this requires $\gamma \sim O(\epsilon^{1/4})$, an assumption that will be used in what follows.

III. NUMERICAL RESULTS

We first introduce a time-dependent sheared frame of reference [19,20] in which the imposed shear flow vanishes. It is defined by the nonorthogonal basis set $\{\mathbf{e}_{x'} = \hat{\mathbf{x}}, \mathbf{e}_{z'} = a(t)\hat{\mathbf{x}} + \hat{\mathbf{z}}\}$ shown in Fig. 1. In this sheared frame, we have the coordinates $x' = x - a(t)z$ and $z' = z$. Also, the corresponding reciprocal basis set is defined as $\{\mathbf{g}_{x'} = \hat{\mathbf{x}} - a(t)\hat{\mathbf{z}}, \mathbf{g}_{z'} = \hat{\mathbf{z}}\}$, with wave vector components expressed as $q_{x'} = q_x$ and $q_{z'} = a(t)q_x + q_z$. After coordinate transformation the Swift-Hohenberg equation (3) becomes

$$\frac{\partial \psi}{\partial t} = \epsilon\psi - (\nabla'^2 + q_0^2)^2\psi - \psi^3, \tag{5}$$

where the modified Laplacian operator takes the form

$$\nabla'^2 = [1 + a^2(t)]\partial_{x'}^2 - 2a(t)\partial_{x'}\partial_{z'} + \partial_{z'}^2.$$

The critical value γ_c for neutral stability is independent of the shear frequency ω and is given by

$$\gamma_c = \left(\frac{-b + \sqrt{b^2 - 4dc}}{2d}\right)^{1/2}, \tag{6}$$

with $b = q_{x'}^2(2\beta^2 + 4q_{x'}^2 - 2q_0^2)/2$, $c = \beta^4 - 2q_0\beta^2 + q_0^4 - \epsilon$, and $d = 3q_{x'}^4/8$ (here $\beta^2 = q_{x'}^2 + q_{z'}^2$). The results for secondary instabilities were already presented in Ref. [19].

We numerically solve Eq. (5) with periodic boundary conditions (in the sheared frame) by using the pseudospectral algorithm described in Ref. [38], and also detailed in the Appendix of Ref. [19]. The equation has been discretized on a 1024×1024 square grid in the sheared frame. In most of our calculations, we choose a mesh spacing $\Delta x' = \Delta z' = \lambda_0/8$, corresponding to eight grid points per wavelength $\lambda_0 (= 2\pi/q_0)$ and so $\Delta q = 1/128$ for the wave number spacing. A second-order, semi-implicit time stepping algorithm is used, with a time step $\Delta t = 0.1$. In order to remain within the weak segregation regime we set $\epsilon = 0.04$ and the angular frequency ω chosen is $O(\epsilon)$. Initial conditions are obtained by numerical solution of Eq. (5) without shear, i.e., $a(t) = 0$, from a starting configuration consisting of two symmetric grain boundaries located at $x' = L_{x'}/4$ and $3L_{x'}/4$ (with $L_{x'} = 1024\Delta x'$ the extent of the system in the x' direction), separating a parallel domain B from two surrounding regions of transverse lamellae. This configuration is allowed to evolve without shear until a stationary solution is reached. This stationary solution is used as the initial condition for the integration with $a(t) \neq 0$.

A. Grain boundary motion due to shear and diffusive relaxation of the order parameter

If $\gamma > \gamma_c = (8\epsilon/3)^{1/4}$, the stability limit of transverse lamellae [Eq. (6)], A lamellae melt to a disordered state ($\psi = 0$), and B lamellae invade region A. If $\gamma < \gamma_c$, but still large enough to result in a secondary instability (Eckhaus, cross-roll, or zigzag) of transverse lamellae at a given frequency (e.g., $\gamma = 0.5$ for $\epsilon = 0.04$ and small ω), our calculations show that small domains of parallel lamellae form within the bulk transverse region A as a result of the instability. These do-

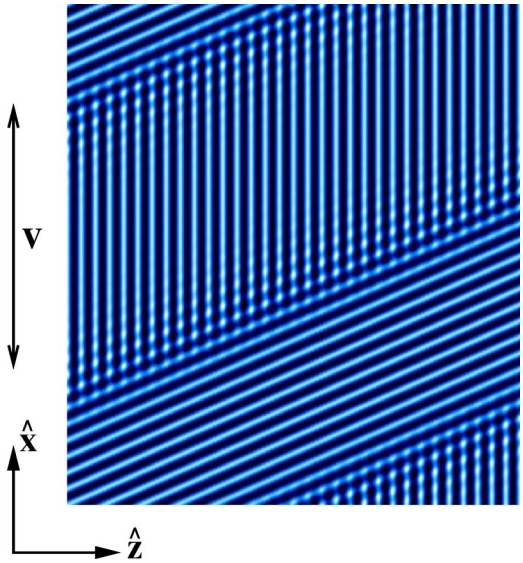

FIG. 2. Grain boundary configuration (in gray scale) at time $t=2.25T_0$ obtained by numerically solving the Swift-Hohenberg equation (5) with $\epsilon=0.04$, $\gamma=0.4$, $\omega=0.04$, and $\Delta x=\lambda_0/32$. The configuration shown here has been transformed back to the laboratory frame $\{\hat{\mathbf{x}},\hat{\mathbf{z}}\}$. As time evolves, the transverse domain is invaded by parallel lamellae, until a uniform parallel configuration occupies the whole system.

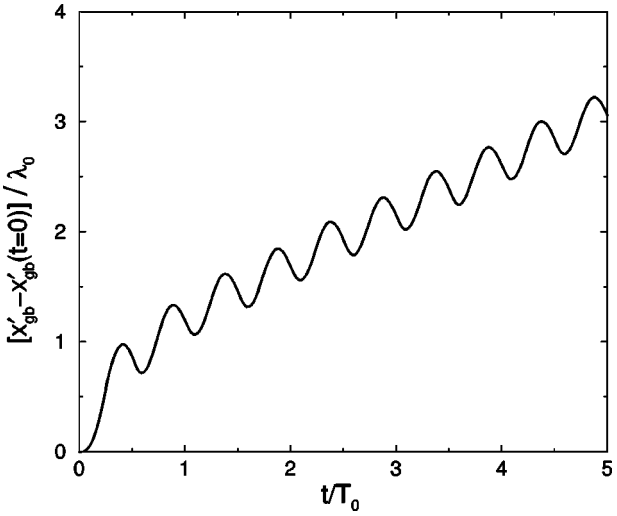

FIG. 3. Relative grain boundary displacement in the sheared frame $[x'_{gb}-x'_{gb}(t=0)]/\lambda_0$ as a function of time t/T_0 for $\epsilon=0.04$, $\gamma=0.4$, $\omega=0.04$, and $\Delta x=\lambda_0/8$.

mains evolve, and connect with each other and with the approaching grain boundary to increase the extent of the parallel region B. In both cases, the final configuration of the system is a uniform lamellar structure of parallel orientation. More interesting phenomena are observed in the range of γ and ω in which both parallel and transverse bulk regions are linearly stable, and when the contributions from shear flow and order parameter diffusion are of the same order, as described at the end of Sec. II. A typical transient configuration in this parameter range is shown in Fig. 2, with $\gamma=0.4$, $\omega=0.04$, and grid spacing $\Delta x=\lambda_0/32$. The configuration shown corresponds to $t=2.25T_0$, where $T_0=2\pi/\omega$ is the shear period, and is presented in the laboratory frame basis set $\{\hat{\mathbf{x}},\hat{\mathbf{z}}\}$.

Our analysis of the transient evolution of the configuration under shear is based on the average location of the grain boundary $\mathbf{x}'_{gb}$. To determine this quantity we use a relation similar to that of Ref. [35]: $B(x'_{gb})=\sqrt{3}\Sigma_{i=1}^{n}[\psi(x'_{gb},i\lambda_0)-\psi(x'_{gb},(i-1/2)\lambda_0)]/4n=\delta$, with n the number of pairs of lamellae in the z' direction, and δ a quantity $O(\epsilon)$. The value used here is $\delta=\epsilon/4$. The grain boundary velocity v'_{gb} is defined as the time rate of change of x'_{gb}. Representative results (in the sheared reference frame) for x'_{gb} and v'_{gb} as a function of time are shown in Figs. 3 and 4. Two distinct features can be clearly distinguished as illustrated in Fig. 2. First, transverse lamellae in the bulk rigidly follow the oscillatory shear flow, leading to a periodic change in their orientation. Second, during part of the cycle the region of parallel lamellae B grows as transverse lamellae in the boundary region break up and reconnect as parallel lamellae (cross-roll instability). This process is partially reversed during the rest of the cycle. The grain boundary exhibits oscillatory motion with a nonzero net average as shown in Figs. 3 (location) and 4 (velocity). Those portions of the shear cycle in which broken transverse lamellae recombine correspond to the segments in Fig. 3 with decreasing x'_{gb}, or negative velocity v'_{gb} in Fig. 4.

Whereas rigid distortion of transverse lamellae is the dominant response to shear in the bulk, order parameter diffusion is important in the boundary region, and is the mechanism that enables dissipation of the excess free energy stored in the bulk transverse region due to shearing. On the one hand, transverse lamellae are elastically compressed by the shear, resulting in a net free energy increase in region A relative to B. As a consequence, the elastic contribution to the system's energy is expected to drive grain boundary motion toward the transverse domain at all times during the shear cycle. On the other hand, backward motion is also observed in Figs. 3 and 4 in those portions of the shear cycle in which the magnitude of the shear strain $a(t)=\gamma\sin(\omega t)$ is small, indicating diffusive relaxation of the order parameter field near the grain boundary. The competition between the two determines the net rate of advance of the boundary. This competition is illustrated in Fig. 4(b) for $\gamma=0.3$ and 0.4 (with the same frequency $\omega=0.01$). By increasing the value of the strain amplitude γ, the relative increase in the peaks of the grain boundary velocity is larger than the decrease in the troughs, thus leading to an increase in average boundary velocity with γ. We also note a decrease in phase lag between the boundary velocity and the imposed shear with γ. The same effect can be seen in Fig. 4(a), as increasing the frequency weakens the effect of diffusion over elasticity.

The net velocity of the average location of the boundary is positive as shown in Figs. 5 and 6. The figures plot the temporal average of velocity over a period $\langle v'_{gb}\rangle=\int_0^{T_0}dt\,v'_{gb}(t)/T_0$ as a function of ω and γ. The velocity increases sharply at very small ω and saturates at large ω. Diffusive relaxation is more pronounced at lower ω, consistent with the calculations shown in Fig. 4(a). $\langle v'_{gb}\rangle$ also depends on strain amplitude γ, as seen in Figs. 5 and 6. The average boundary velocity increases approximately as $\langle v'_{gb}\rangle\sim\gamma^{\alpha}$ with $\alpha\sim4$. The range of strain amplitude accessible to

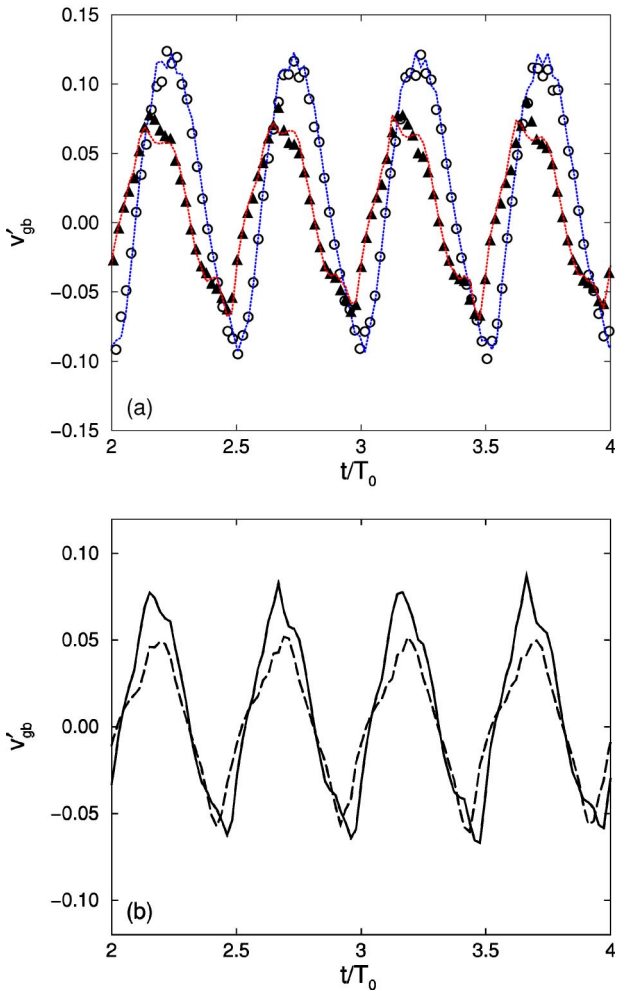

FIG. 4. Boundary velocity v'_{gb} as a function of time obtained from direct numerical integration of Eq. (5) with $\epsilon=0.04$ and different values of ω and γ. (a) Fixed strain amplitude $\gamma=0.4$, $\omega=0.01$ (filled triangles), and $\omega=0.04$ (open circles). The dotted lines are the corresponding results obtained from numerical integration of the amplitude equations (10) and (11). (b) Results at constant frequency $\omega=0.01$, but different strain amplitudes $\gamma=0.4$ (solid line) and 0.3 (dashed line).

our calculations is limited by the restriction that $\gamma \sim O(\epsilon^{1/4})$. As discussed above, the transverse lamellar region is unstable for larger γ, whereas for smaller γ, diffusion of order parameter dominates. Note that the power law dependence is consistent with experiments in PS-PI copolymers [8,11], in which the rate of global alignment of a bulk sample is a power law of the strain amplitude, with an exponent in the range 3–5.

B. Wave number adjustment in the transverse region

Bulk transverse lamellae elastically compressed by the shear would have a wave number $q_0\sqrt{1+a^2(t)}$ in the laboratory frame, or $q_{x'}=q_0$, constant, in the sheared frame. Order parameter diffusion in the boundary region, however, is seen to lead to a wave number modification of transverse lamellae relative to what would be expected from rigid deformation.

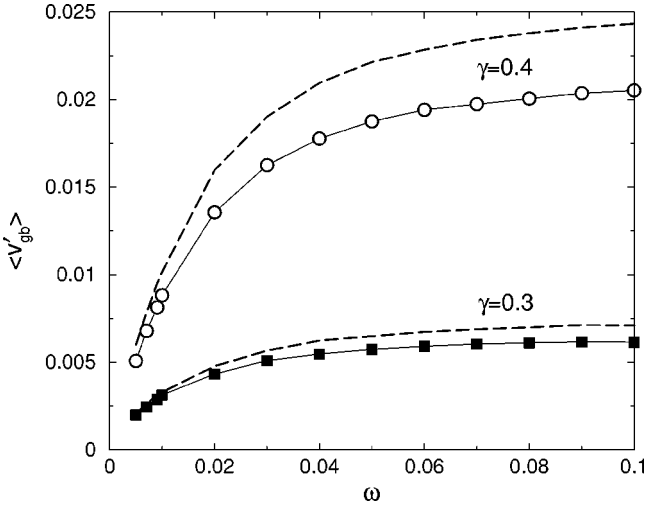

FIG. 5. Temporal average of the grain boundary velocity $\langle v'_{gb}\rangle$ as a function of frequency ω. The symbols correspond to the solution of the order parameter model, Eq. (5), for $\gamma=0.4$ (circles) and 0.3 (squares), while the corresponding dashed lines are obtained from the amplitude equations (10) and (11).

We show in Fig. 7 the structure factor $|\psi_{q_{x'}}|$ along the x' direction defined as the Fourier transform of the order parameter ψ at fixed z' (e.g., at $z'=L_{z'}/2$, with $L_{z'}=1024\Delta z'$ the system size along z' direction). For large enough $\gamma(\gamma>0.1)$, the peak in $|\psi_{q_{x'}}|$ shifts away from $q_0=1$ with time, asymptotically reaching a constant $q^m_{x'}<q_0$ [Fig. 7(a)]. We have studied this wave number compression for different frequencies ω and strain amplitudes γ. We find that the value of $q^m_{x'}$ is independent of ω, but that it increases with decreasing γ [Fig. 7(b)]: $\delta q^m_{x'}=q_0-q^m_{x'}=5\Delta q$ (with $\Delta q=1/128$) for $\gamma=0.4$ (solid line), $\delta q^m_{x'}=3\Delta q$ for $\gamma=0.3$ (dotted line), $\delta q^m_{x'}=\Delta q$ for $\gamma=0.2$ (dashed line), and $\delta q^m_{x'}=0$ for $\gamma=0.1$ (thin solid line). These values correspond to the disappearance of

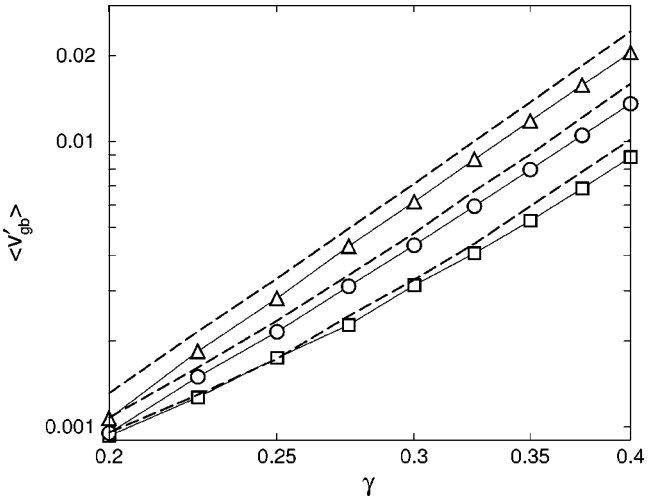

FIG. 6. Log-log plot of average velocity $\langle v'_{gb}\rangle$ vs strain amplitude γ for $\omega=0.01$ (squares), 0.02 (circles), and 0.1 (triangles) from direct solution of Eq. (5). Also shown (dashed lines) are the corresponding results given by the amplitude equations (10) and (11).

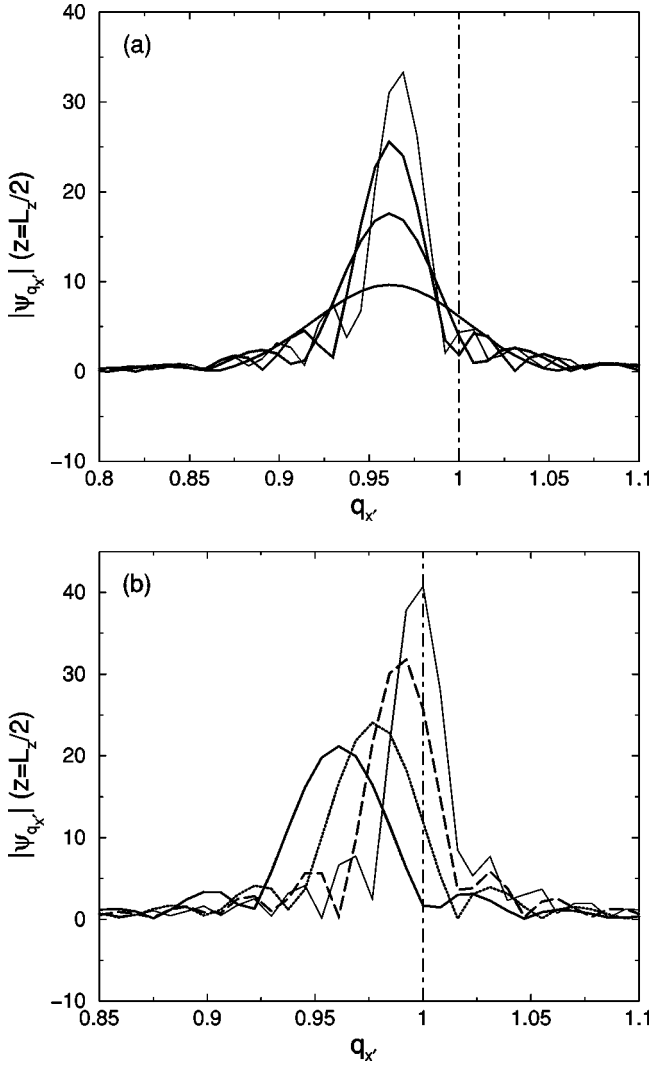

FIG. 7. One-dimensional structure factor for transverse lamellae $|\psi_{q_{x'}}|$ along the x' direction at $z'=L_{z'}/2$ as a function of wave number $q_{x'}$. (a) Different times from top to bottom: $30T_0$, $40T_0$, $50T_0$, and $60T_0$ with $\gamma=0.4$ and $\omega=0.04$. (b) Different strain amplitudes: $\gamma=0.4$ and $t=100T_0$ (solid curve), $\gamma=0.3$ and $t=300T_0$ (dotted curve), $\gamma=0.2$ and $t=1200T_0$ (dashed curve), and $\gamma=0.1$ and $t=12\,000T_0$ (thin solid curve). Here $\omega=0.1$, and $\Delta t=0.1$ except for $\gamma=0.1$ in which case we have used $\Delta t=0.2$. In both cases (a) and (b), the vertical dot-dashed line indicates the location of the wave number $q_{x'}=q_0=1$.

5, 3, 1, and 0 lamellae in region A respectively. We further discuss this finding in Sec. IV, and in the discussion in Sec. V. In addition to the motion in the position of the peak of the structure factor, Fig. 7(a) also shows a decreasing amplitude and broadening of the peak. This is due to the finite size of the configuration; as the grain boundary moves, the region occupied by transverse lamellae decreases.

The power spectrum of region B $|\psi_{q_{z'}}|$ as a function of $q_{z'}$ (the Fourier transform of ψ at fixed x' position, results not shown here) is unaffected by the shear flow. Its maximum is located at $q_z=q_{z'}=q_0$, without any visible shift in time.

IV. MULTIPLE SCALE ANALYSIS AND AMPLITUDE EQUATIONS

A multiple scale analysis of the type frequently used to derive amplitude equations close to instability thresholds [31,32,34,39] can be introduced here to derive an equation of motion for the grain boundary in the limit of weak segregation $\epsilon \ll 1$. As shown in Fig. 1, we first define a time-dependent, orthogonal basis set $\{\mathbf{e}_{x_A}=[\hat{\mathbf{x}}-a(t)\hat{\mathbf{z}}]/[1+a^2(t)], \mathbf{e}_{z_A}=[a(t)\hat{\mathbf{x}}+\hat{\mathbf{z}}]/[1+a^2(t)]\}$ (different from the nonorthogonal sheared frame $\{\mathbf{e}_{x'}, \mathbf{e}_{z'}\}$ used in Sec. III). This frame is the orthogonal frame of reference attached to the transverse region. The corresponding coordinates are $x_A=x-a(t)z$ and $z_A=a(t)x+z$. We then introduce an anisotropic coordinate scaling to define slowly varying amplitudes of $\exp(iq_0x_A)$ as $X_A=\epsilon^{1/2}x_A$ and $Z_A=\epsilon^{1/4}z_A$. The derivation of these scaling forms follows the method of Ref. [31] by considering a slow modulation of a lamellar pattern such that $q_{x_A}\sim q_A+\delta q_{x_A}$ $[q_A=q_0\sqrt{1+a^2(t)}]$ and $q_{z_A}\sim \delta q_{z_A}$ for wave vector components along and perpendicular to the lamellar normal (see Fig. 1). Consistency in the expansion of Eq. (3) requires $(\nabla^2+q_0^2)^2\sim\epsilon$ and thus $[(1+a^2)(q_{x_A}^2+q_{z_A}^2)-q_0^2]^2\sim\epsilon$, leading to $\delta q_{x_A}\sim\delta q_{z_A}^2\sim O(\epsilon^{1/2})$, as well as to the above anisotropic scaling. We retain the laboratory frame coordinates in region B, $\{\hat{\mathbf{x}},\hat{\mathbf{z}}\}$, with a base mode given by $\exp(iq_0z)$. Its slowly varying amplitude is a function of the rescaled variables $X_B=\epsilon^{1/4}x$ and $Z_B=\epsilon^{1/2}z$, with the scaling forms different from those of region A due to the different lamellar orientation. We then expand the order parameter field ψ as

$$\psi=\frac{1}{\sqrt{3}}(Ae^{iq_0x_A}+Be^{iq_0z}+\text{c.c.}), \tag{7}$$

where both complex amplitudes A and B are functions of the slow spatial scales X_A, Z_A, X_B, and Z_B, and of a slow time scale $T=\epsilon t$. The requirement of slow amplitude change restricts our analysis to low frequencies $\omega\sim O(\epsilon)$, and we further focus on sufficiently small shear amplitudes so that advection and local diffusion balance. This requires $\mathbf{v}\cdot\boldsymbol{\nabla}=(da/dt)z\partial_x\sim(\boldsymbol{\nabla}^2+q_0^2)^2\sim\epsilon$ according to Eq. (3). Considering that in the transverse region $\partial_x=\partial_{x_A}+a\partial_{z_A}$, $\partial_z=-a\partial_{x_A}+\partial_{z_A}$, $z=(-ax_A+z_A)/(1+a^2)$, as well as the spatial (x_A,z_A) and temporal scalings, we require that $\gamma\sim O(\epsilon^{1/4})$. The same relationship follows from the scalings appropriate for the parallel region.

Following standard multiple scale procedure [32,34], we introduce the expansions $\partial_x\to\partial_{x_A}+\epsilon^{1/4}\partial_{X_B}+\epsilon^{1/2}(\partial_{X_A}+\bar{a}\partial_{Z_A})$, $\partial_z\to\partial_z+\epsilon^{1/4}(-\bar{a}\partial_{x_A}+\partial_{Z_A})+\epsilon^{1/2}\partial_{Z_B}-\epsilon^{3/4}\bar{a}\partial_{X_A}$, and $\partial_t+(da/dt)z\partial_x\to\epsilon[\partial_T+\dot{\gamma}_\Omega(X_A\partial_{Z_A}+Z_B\partial_{X_B})]+O(\epsilon^{5/4})$ (here $\bar{a}$ and $\dot{\gamma}_\Omega$ are defined by $a=\epsilon^{1/4}\bar{a}$ and $da/dt=\epsilon^{5/4}\dot{\gamma}_\Omega$), and we derive the following amplitude equations at $O(\epsilon^{3/2})$ from Eq. (3):

$$\partial_tA=\left[\epsilon-\frac{da}{dt}x_A\partial_{z_A}-(2iq_0\partial_{x_A}+\partial_{z_A}^2-q_0^2a^2)^2\right]A - |A|^2A-2|B|^2A, \tag{8}$$

$$\partial_t B = \left[\epsilon - \frac{da}{dt} z\partial_x - (\partial_x^2 + 2iq_0\partial_z)^2 \right] B - |B|^2 B - 2|A|^2 B. \tag{9}$$

For $\gamma=0$, these equations reduce to those of Refs. [33,34].

Equations (8) and (9) are expressed in two different coordinate systems. We next transform them to a common sheared frame $\{\mathbf{e}_{x'}, \mathbf{e}_{z'}\}$, by using the relations $x_A = x'$ and $z_A = ax' + (1+a^2)z'$. The base state of the order parameter is still given by Eq. (7) (with x_A replaced by x'), and to $O(\epsilon^{3/2})$, the resulting 2D amplitude equations were already given in Ref. [40]. Here we further assume a planar grain boundary in the sheared frame, for which the dependence of the amplitudes on the coordinate z' parallel to the grain boundary can be ignored. The complex amplitudes A and B satisfy the 1D equations

$$\partial_t A = [\epsilon - (2iq_0\partial_{x'} - q_0^2 a^2)^2] A - |A|^2 A - 2|B|^2 A, \tag{10}$$

and

$$\partial_t B = [\epsilon - (2iq_0 a\partial_{x'} - \partial_{x'}^2)^2] B - |B|^2 B - 2|A|^2 B. \tag{11}$$

At $O(\epsilon^{3/2})$, two contributions from the shear flow remain in Eqs. (10) and (11). The first one involves the term $-2iq_0 a\partial_{x'}$ in Eq. (11) and the term $(q_0^2 a^2)(2iq_0\partial_{x'})$ obtained from the expansion of Eq. (10), which is non-negligible only in the grain boundary region and leads to diffusive relaxation of the order parameter. The second is $q_0^4 a^4 A$ in Eq. (10). This term is uniform in the entire region A and reflects the contribution from advection of transverse lamellae by the flow.

We had analytically calculated the velocity of the grain boundary from these amplitude equations in Ref. [40] by assuming that the amplitudes can be approximated by $A(x',t) \simeq A(x' - x'_{\rm gb}(t))$ and $B(x',t) \simeq B(x' - x'_{\rm gb}(t))$. We found that the velocity is proportional to the free-energy difference between the transverse and parallel phases, in agreement with previous studies in the absence of flow [29,33,35]. Also, the results gave the correct order of magnitude of the average velocity, but we noted quantitative discrepancies [40]. We argued that the adiabatic approximation for $A(x',t)$ and $B(x',t)$ given cannot incorporate diffusive relaxation of the order parameter in the boundary region so that the calculation only yields an upper bound to the net boundary velocity. Since we have argued in Sec. III that this relaxation is important, we turn here to a numerical determination of the boundary velocity.

We present next the results of the numerical solution of Eqs. (10) and (11). We initially consider a region of parallel lamellae B surrounded by two regions of transverse lamellae A, and use periodic boundary conditions in the integration. Both amplitudes A and B are complex variables. A pseudospectral method is applied, with a Crank-Nicholson scheme used for the linear terms, and a second-order Adams-Bashford scheme used for the nonlinear terms. The instantaneous location of the grain boundary $x'_{\rm gb}(t)$ is defined by the condition $|B(x'_{\rm gb})| = \epsilon/4$, and its velocity $v'_{\rm gb}$ is found by taking the time derivative of $x'_{\rm gb}(t)$. In order to compare with the 2D results of the original model shown in Sec. III, we set the system size $L=1024$, the time step $\Delta t = 0.1$, and the grid spacing $\Delta x' = \lambda_0/8$. As was the case there, the initial condition for A and B is provided by the steady solution of the amplitude equations in the absence of shear. Our results for the boundary velocity for $\gamma=0.4$, $\omega=0.01$, and $\omega=0.04$ are shown as dotted curves in Fig. 4(a), both in good agreement with the direct solution of original model equation (5) (symbols in the figure). The time averaged velocity $\langle v'_{\rm gb} \rangle$ is shown by the dashed lines in Figs. 5 and 6.

In order to further analyze the wave number readjustment process discussed in Sec. III B, we show our results in terms of the phase ϕ_A of the complex amplitude A. In the sheared frame we define $A = |A| \exp(i\phi_A)$ and plot ϕ_A as a function of grid index $i_{x'} = x'/\Delta x'$ in Fig. 8. Near the boundary, the phase becomes linear in space: $\phi_A \propto -\delta q x'$ [the linear behavior is clearer for a larger system size, as seen by comparing Fig. 8(a) ($L=1024$) with Fig. 8(b) ($L=4096$)], indicating a local wave number change $q_{x'} \to q_0 - \delta q$. This is also in agreement with the direct solution of the original model as shown in Fig. 7. Note also that the region of linearity (right side of dot-dashed line in Fig. 8) increases with time, indicating that the readjustment of the local wavelength of the transverse lamellae first occurs at the boundary and then progressively propagates into the bulk. At late times [e.g., $t = 40T_0$ in Fig. 8(a)], the wave number change can be observed in the whole transverse domain, with $q_{x'}$ corresponding to the stationary peak position of the structure factor $|\psi_{q_{x'}}|$ presented in Fig. 7(a) ($t \geqslant 40T_0$ there). We find that $\delta q = \delta q^m_{x'}$, the wave number shift discussed in Sec. III, by determining δq from the slope of the dotted line in Figs. 8(a) and 8(b).

V. DISCUSSION AND CONCLUSIONS

A coarse-grained order parameter model has been used to study the motion of a grain boundary separating two regions of uniform parallel and transverse lamellae under an imposed shear flow. The motion of the boundary is oscillatory, and the driving force for motion is the excess energy stored in the elastically strained transverse phase that can only be relieved through diffusive relaxation of the order parameter in the boundary region. Diffusive relaxation, however, is complex as the response of the order parameter field is out of phase with the shear, and lamellae break up and reconnect during each of the cycles. As expected, the effects of diffusive relaxation are more pronounced for small shear strain and low angular frequency, as seen in both the time-dependent behavior of boundary velocity (Fig. 4) or the time averaged velocity (Figs. 5 and 6). Although under the conditions of the study both transverse and parallel orientations are linearly stable, we observe net motion of the boundary toward the region occupied by transverse lamellae.

As the boundary moves over time, we have observed that the wave number of the transverse lamellae does not remain constant and equal to q_0. Instead, it is slowly readjusted by wave number diffusion, as shown by both direct solution of

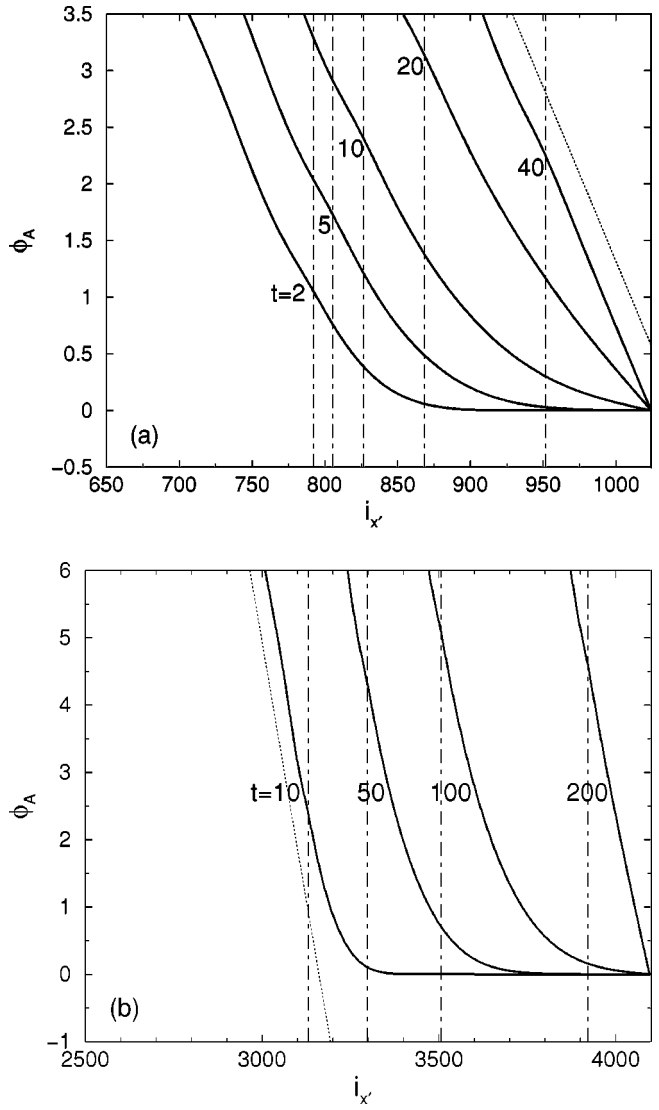

FIG. 8. Phase ϕ_A of the complex amplitude A as a function of position in the sheared frame (in terms of the grid index $i_{x'}$) with $\Delta x' = \lambda_0/8$, $\gamma = 0.4$, and $\omega = 0.04$. Two system sizes are shown: (a) $L = 1024$ at times (from left to right) $t = 2T_0$, $5T_0$, $10T_0$, $20T_0$, and $40T_0$ [to be compared with Fig. 7(a)]; and (b) $L = 4096$ at times (from left to right) $t = 10T_0$, $50T_0$, $100T_0$, and $200T_0$. The vertical dot-dashed lines indicate the instantaneous grain boundary positions $x'_{\rm gb}$, and a dotted line with slope $-\delta q^m_{x'} \Delta x' = -5\Delta x'/128$ is also shown for reference.

the coarse-grained model of Sec. III and the corresponding complex amplitude equations of Sec. IV. The wave number shift $\delta q^m_{x'}$ is approximately independent of shear frequency ω, but strongly dependent on the strain amplitude γ. In order to understand the physical origin of wave number compression (or lamellae expansion) that occurs in the transverse region A, we focus on the lamellae near the grain boundary, since the calculation in Sec. IV shows that wave number change is initiated at the boundary and then it propagates into the bulk. Since the amplitude of the transverse lamellae goes to zero at the boundary region, it is possible to create or eliminate lamellar planes there in a way that is not possible in the bulk for the parameters of our study [19]. First, consider the stability diagram of the Swift-Hohenberg model (3) at zero shear [41]. For fixed ϵ and $q_x > q_0$, the closest instability boundary in the q_x-ϵ diagram is the Eckhaus instability given by

$$\epsilon = 12(q_x - q_0)^2. \tag{12}$$

For $\epsilon = 0.04$ and $q_0 = 1$, we have the Eckhaus boundary at $q_x^{\rm E} = q_0 + (\epsilon/12)^{1/2} = 1.0577$. In our case q_x is the wave number of the transverse lamellae in the lab frame, and equal to $q_0\sqrt{1+a^2(t)}$ if we assume that the lamellae are rigidly distorted by the shear. The maximum value of q_x is then $q_x^{\rm max} = q_0\sqrt{1+\gamma^2}$ so that for $\gamma = 0.4$ we have $q_x^{\rm max} > q_x^{\rm E}$. Although this is not sufficient to destabilize the bulk transverse region (according to the stability diagrams in Ref. [19] obtained by Floquet analysis over the entire period of the oscillation), it appears to be sufficient to induce lamellar elimination at the grain boundary region, as seen in Figs. 7 and 8. The figures show that $\delta q^m_{x'} = 5\Delta q$, corresponding to the elimination of five transverse lamellae. As γ decreases $q_x^{\rm max}$ also decreases, becoming smaller than $q_x^{\rm E}$, and eventually lamellae elimination is expected to cease. This is consistent with our results shown in Fig. 7(b). With decreasing value of γ from 0.4 to 0.1, the number of lost transverse lamellae decreases from 5 to 0.

In summary, for small shear strains and low frequencies such that diffusion of order parameter is of the same order as advection by the flow, the excess free energy in the transverse region relative to the marginal parallel region is dissipated through order parameter diffusion in the grain boundary region. The latter includes break up and reconnection of transverse lamellae, and a weak Eckhaus instability developing at the grain boundary that diffuses into the bulk transverse lamellae leading to dynamical wave number readjustment. A weakly nonlinear analysis, as well as the amplitude equations derived, capture quantitatively all aspects of grain boundary motion, including the boundary velocity and the wave number readjustment. The order parameter distribution in the boundary region can be represented crudely by introducing an adiabatic approximation into the amplitude equations, which gives a reasonable approximation to the net boundary velocity toward the transverse region, and be well reproduced by the direct solution of the amplitude equations. Although our study is confined to the case of a transverse/parallel grain boundary in two dimensions, we expect that our results will qualitatively hold for both three-dimensional transverse/parallel and transverse/perpendicular cases. In three dimensions, however, there is a completely different type of tilt boundary, that between parallel and perpendicular lamellae. Both orientations are marginal with respect to the shear. This configuration is currently under investigation.

ACKNOWLEDGMENT

This work was supported by the National Science Foundation under Grant No. DMR-0100903.

[1] G. H. Fredrickson and F. S. Bates, Annu. Rev. Mater. Sci. **26**, 501 (1996).
[2] R. G. Larson, *The Structure and Rheology of Complex Fluids* (Oxford University Press, New York, 1999).
[3] A. Keller, E. Pedemonte, and F. M. Willmouth, Kolloid Z. Z. Polym. **238**, 385 (1970); Nature (London) **225**, 538 (1970).
[4] G. Hadziioannou, A. Mathis, and A. Skoulios, Colloid Polym. Sci. **257**, 136 (1979).
[5] K. A. Koppi, M. Tirrell, F. S. Bates, K. Almdal, and R. H. Colby, J. Phys. II **2**, 1941 (1992).
[6] K. I. Winey, S. S. Patel, R. G. Larson, and H. Watanabe, Macromolecules **26**, 2542 (1993).
[7] U. Wiesner, Macromol. Chem. Phys. **198**, 3319 (1997); D. Maring and U. Wiesner, Macromolecules **30**, 660 (1997).
[8] Z.-R. Chen and J. A. Kornfield, Polymer **39**, 4679 (1998).
[9] I. W. Hamley, J. Phys.: Condens. Matter **13**, R643 (2001).
[10] B. S. Pinheiro, D. A. Hajduk, S. M. Gruner, and K. I. Winey, Macromolecules **29**, 1482 (1996).
[11] V. K. Gupta, R. Krishnamoorti, Z.-R. Chen, J. A. Kornfield, S. D. Smith, M. M. Satkowski, and J. T. Grothaus, Macromolecules **29**, 875 (1996).
[12] D. L. Polis and K. I. Winey, Macromolecules **31**, 3617 (1998); L. Qiao and K. I. Winey, *ibid.* **33**, 851 (2000).
[13] Z.-R. Chen, A. M. Issaian, J. A. Kornfield, S. D. Smith, J. T. Grothaus, and M. M. Satkowski, Macromolecules **30**, 7096 (1997).
[14] L. Leibler, Macromolecules **13**, 1602 (1980).
[15] T. Ohta and K. Kawasaki, Macromolecules **19**, 2621 (1986).
[16] G. H. Fredrickson and E. Helfand, J. Chem. Phys. **87**, 697 (1987).
[17] M. E. Cates and S. T. Milner, Phys. Rev. Lett. **62**, 1856 (1989).
[18] G. H. Fredrickson, J. Rheol. **38**, 1045 (1994).
[19] F. Drolet, P. Chen, and J. Viñals, Macromolecules **32**, 8603 (1999).
[20] P. Chen and J. Viñals, Macromolecules **35**, 4183 (2002).
[21] T. Ohta, Y. Enomoto, J. L. Harden, and M. Doi, Macromolecules **26**, 4928 (1993).
[22] H. Kodama and M. Doi, Macromolecules **29**, 2652 (1996).
[23] S. R. Ren, I. W. Hamley, P. I. C. Teixeira, and P. D. Olmsted, Phys. Rev. E **63**, 041503 (2001).
[24] A. N. Morozov, A. V. Zvelindovsky, and J. G. E. M. Fraaije, Phys. Rev. E **64**, 051803 (2001); A. N. Morozov and J. G. E. M. Fraaije, Phys. Rev. E **65**, 031803 (2002).
[25] A. V. Zvelindovsky, G. J. A. Sevink, B. A. C. van Vlimmeren, N. M. Maurits, and J. G. E. M. Fraaije, Phys. Rev. E **57**, R4879 (1998).
[26] S. R. Ren, I. W. Hamley, A. V. Zvelindovsky, G. J. A. Sevink, and J. G. E. M. Fraaije, Macromol. Theory Simul. **11**, 123 (2002).
[27] M. Bahiana and Y. Oono, Phys. Rev. A **41**, 6763 (1990).
[28] D. Boyer and J. Viñals, Phys. Rev. E **64**, 050101(R) (2001).
[29] D. Boyer and J. Viñals, Phys. Rev. E **65**, 046119 (2002).
[30] Y. Yokojima and Y. Shiwa, Phys. Rev. E **65**, 056308 (2002).
[31] P. Manneville, *Dissipative Structures and Weak Turbulence* (Academic Press, New York, 1990).
[32] M. C. Cross and P. C. Hohenberg, Rev. Mod. Phys. **65**, 851 (1993).
[33] P. Manneville and Y. Pomeau, Philos. Mag. A **48**, 607 (1983).
[34] G. Tesauro, and M. C. Cross, Philos. Mag. A **56**, 703 (1987).
[35] D. Boyer and J. Viñals, Phys. Rev. E **63**, 061704 (2001).
[36] G. H. Fredrickson and K. Binder, J. Chem. Phys. **91**, 7265 (1989).
[37] J. Swift and P. C. Hohenberg, Phys. Rev. A **15**, 319 (1977).
[38] M. C. Cross, D. Meiron, and Y. Tu, Chaos **4**, 607 (1994).
[39] A. C. Newell and J. A. Whitehead, J. Fluid Mech. **38**, 279 (1969); L. A. Segel, J. Fluid Mech. **38**, 203 (1969).
[40] Z. F. Huang, F. Drolet, and J. Viñals, Macromolecules **36**, 9622 (2003).
[41] H. S. Greenside and W. M. Coughran, Jr., Phys. Rev. A **30**, 398 (1984).